A case study on heat source mechanism of high-temperature geothermal field

Junjie Ba*, Chuntian Su, Yanqing li

Key Laboratory of Karst Dynamics, MLR & GZAR,
Institute of Karst Geology, CAGS, Guilin, 541004, China

bajunjie@kmust.edu.cn

ABSTRACT. *The heat source mechanism is vital to the activity of high-temperature geothermal field. This paper analyses the intrusion era, scale and temperature of magma chamber and the radiation heat of basal granite in Ruidian geothermal field, a typical constrained heat source dominated by magma chamber in southwestern China. The analysis results show that: an intrusive high-temperature magma chamber was formed in Late Pleistocene in Gudong-Mazhan Belt, southern Yunnan Province; the magma chamber was an approximate ellipsoid with a 19km-long east-west axis, a 25km-long north-south axis, a 15km-height, and a highest temperature of 700°C. The basement of this geothermal field is biotite adamellite rich in radioactive elements (e.g. 238U, 232Th and 40K). The mean decay heat generation rate stands at 6.90μW/m³ and the estimated temperature is 116~120°C at the depth of 2km. In addition, the said magma chamber is the main heat source, whose radiogenic heat contributes to the temperature distribution of Ruidian high-temperature geothermal field. In this way, the author discovered the formation mechanism of Ruidian high temperature geothermal field, laying a solid basis for further research on heat source mechanism of geothermal fields.*

RÉSUMÉ. *Le mécanisme de source de chaleur est essentiel à l'activité du champ géothermique à haute température. Cet article analyse l'époque de l'intrusion, l'échelle et la température de la chambre magmatique et la chaleur de radiation du granite basal dans le champ géothermal de Ruidian, une source de chaleur contrainte typique dominée par la chambre magmatique dans le sud-ouest de la Chine. Les résultats de l'analyse montrent que: une chambre magmatique intrusive à haute température s'est formée au Pléistocène supérieur dans la zone de Gudong – Mazhan, dans le sud de la province du Yunnan; la chambre magmatique était un ellipsoïde approximatif avec un axe est-ouest de 19 km de long, un axe nord-sud de 25 km, une hauteur de 15 km et une température maximale de 700°C. Le sous-sol de ce champ géothermique est constitué d'adamellite biotite riche en éléments radioactifs (par exemple 238U, 232Th et 40K). Le taux moyen de génération de chaleur de désintégration est de 6,90 μW/m³ et la température estimée est de 116~120°CC à une profondeur de 2 km.En outre, ladite chambre magmatique est la principale source de chaleur, dont la chaleur radiogénique contribue à la répartition de la température du champ géothermique à haute température de Ruidian. De cette façon, l'auteur a découvert le mécanisme de formation du champ géothermique à haute température de Ruidian, posant ainsi une base solide pour la poursuite des recherches sur le mécanisme de source de chaleur des champs géothermiques.*

Annales de Chimie - Science des Matériaux – n° 1/2018, 129-147

KEYWORDS: geothermal field, heat source, magma chamber, granite radioactivity, ruidian, China.

MOTS-CLÉS: champs géothermiques, source de chaleur, la chambre magmatique, Radioactivité des granits Ruidian, a chine.

DOI:10.3166/ACSM.42.129-147 © 2018 Lavoisier

1. Introduction

Geothermal is a kind of green energy and it consists heat, mine and water. It wins popularity with its wide coverage, low-polluting to ecological environment, low operation costs. The exploiting researches of geothermal bloom to a brighter future (Guo, 2012; Wang *et al.,* 2000). China has the second largest reserves in the world, which can be well developed and utilized. There are four hydrothermal activity concentrated belts in China: Southern Tibet-Western Yunnan, Taiwan, Southeast coast of China and Jiaodong-Liaodong peninsula. Viewing from geological structure, most Chinese geothermal resources are distributed in tectonic norbile belts and large sedimentary basins (Guo *et al.,* 2013; Pang *et al.,* 2012; Zeng *et al.,* 2010).

In China, the high temperature geothermal fields related to magmatism are mainly located in Yunan-Tibet area, particularly Yangbajing geothermal field in the south of Hengduan Moutains, Rehai and Ruidian geothermal fields in Tengchong. These geothermal fields generate high temperature hot springs and strong hydrothermal activities. There is uncondensed intrusive mass or high temperature molten magma chamber in the underlying strata of the above geothermal fields. They are the heat sources to maintain these high temperature geothermal fields. Moreover, the rediation heat produced by base granite is also an indispensable heat source to these fields.

Researchers have studied the relationship between magma chambers and high temperature geothermal fields. In 2003, Wilson. CK used teleseism-ray seismograms to analyze the Coso geothermal field near Ridgecrest, CA, USA, and found that shallow source magma chamber has a significant impact on the temperature of that geothermal field (Wilson *et al.,* 2003). In 2014, Piña-Varas *et al.* used 3D magnetoelluric exploration (MET) studied Tenerife geothermal field in Spain's Canary Islands, and found that the underlying magma chamber is the main heat source to that geothermal field (Piña-Varas *et al.,* 2014).

Researchers also studied the radiation heat of granite in large high temperature Hot Dry Rock (HDR) areas. In 2010, Tenzer *et al.* used EGS mode to design and exploit the HDR area of Soultz-sous-Forts, France and Spa Urach, Germany. They obtained the key parameters of heat transfers between reservoir fluid and granite (Tenzer *et al.,* 2010). In 2015, Abul *et al.* investigated the hear generation rate of granite in Cooper basin, central of South Australia. Theses researches concluded that the high concentrations of ^{238}U, ^{232}Th and ^{40}K in granite lead to the high temperature of these geothermal fields in HDR areas (Khair *et al.,* 2010).

In summary, the predecessors have studied the high temperature geothermal field dominated by magma chamber heat source and granite Hot Dry Rock (HDR) to some extent, but there are few systematic and comprehensive studies on the formation conditions and genetic model of magma chamber dominant constrained heat source. Therefore, studying and analyzing the heat source mechanism of Ruidian high temperature geothermal field, will be important basis and provide guidance to the researches of other similar geothermal fields and high temperature hot springs. In addition, our research can also provide a guidance to evaluate the prospect of this kind high temperature geothermal resource, and exploit them reasonably.

2. Geological setting

Tengchong County is China's southwestern border in Baoshan, Yunnan province. Ruidian geothermal field is 50 km to the north of Tengchong, 25°22′-25°30′ N and 98°23′-98°30′ E (Figure 1a). Ruidian geothermal field, located in Southern Tibet-Western Yunnan hydrothermal activity concentrated belt, is a typical representative of magma chamber dominant constrained heat source. Its cause is ralated to geological setting, fault zone and magma chamber activities, ect. It is formated at the same era as Nabang Fault, Dayingjiang River Fault and Nujiang River Fault.

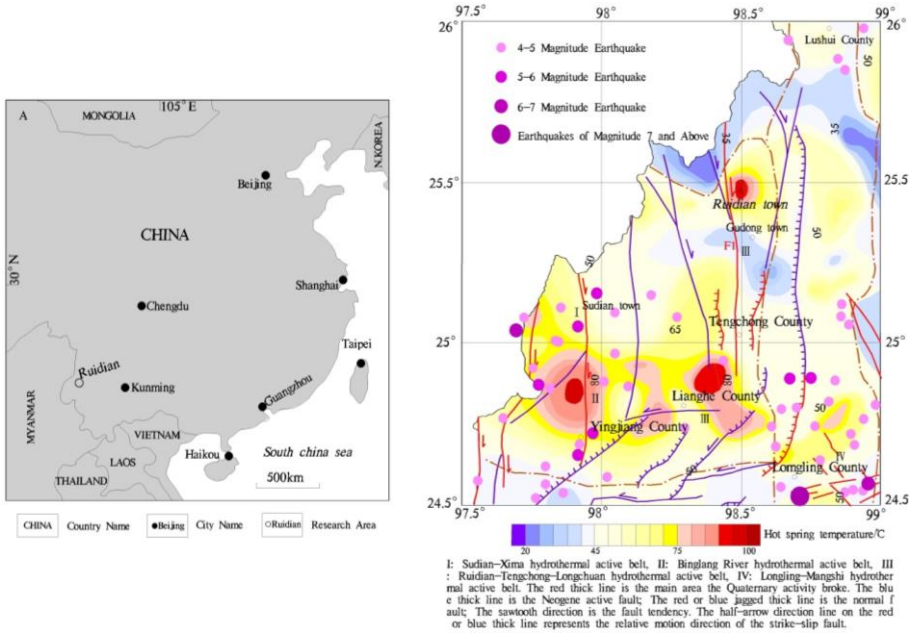

(a) (b)

Figure 1. (a) The location of Ruidian gerothermal field and (b) Hydrothermal activity distribution of Ruidian gerothermal field

Ruidian geothermal field is located in Ruidian-Tengchong-Longchuan hyrothermal activity belt (Figure 1b). There is a large area of Lower Proterozoic Gaoligongshan Group metamorphic rocks distribute in the south and east of this belt, while Yanshanian granite and Cenozoic volcanic rocks distribute in the north and west. The general hydrothermal activites in the surface are boiling springs, steaming grounds, fumaroles and sinters. There are about 59 hot springs higher than 45℃, among which Ruidian, Rehai and Ruili are the most famous in China (Fiture 1b).

Ruidian geothermal field is located where the northward extension Dayingjiang River-Tengchong Fault (F1) and Ruidian-Qushi Fault meet (Fiture 1b). Ruidian basin is foundmentally formulated in Yanshanian by lava-dam intrusion. In the beginning of Himalayaorogeny, the crustal uplift strongly to form moutains and valleys in this belt. There are 39 hot springs discovered in Ruidian geothermal field. Most of them are spring groups and the highest temperature can reach 91.5 °C. The geothermal reservoir structure can be divided to high temperature deep granite weathering bed and shallow Low Pleistocene gravel and pebble bed.

3. Geothermal-controlling of magma chamber

3.1. Characteristics of ground temperature field

The value of heat flow in Ruidian ground temperature field is generally high. For example, the terrestrial heat flow in Tengchong-Ruidian belt can reach 120.5 mW/m^2, which is double to the global average velue (61.6 mW/m^2) (Zhou, 1997). Although the terrestrial heat flows in Zhenan and Luxi of Longling County, which are far from the heat center in Tengchong, decrease to 73-77 mW/m^2, the average velue of the whole Tengchong zone (91 mW/m^2) is about 1.5 times to the global average velue. The crustal heat flow (q_c) in Yunnan is generally of 30-47 mW/m^2. However, the mantle heat flow (q_m) in Tengchong area is 56.4 mW/m^2-the highest value in Yunnan province (Zhou,1997). The high heat flow in Tengchong is due to the magma's residual heat caused by volcano activities in neoid period.

The temperature of Moho of Ruidian geothermal field can reach 1140 °C (Xu *et al.*, 1997). The ratios of mantle heat flow (q_m)/earth surface heat flow (q_s), q_m/q_c and q_c/q_m are 60.4, 1.53-1.63 and 0.61-0.66, respectively (Zhou *et al.*, 1997). The above characteristics indicate that Tengchong is an anomalous high temperature geothermal zone of strong modern tectonic activities.

3.2. Distribution characteristics of magma chamber

In Early Pliocene, the depression in Tengchong volcanic rock area provided suitable basic geological structure conditions for the eruption of these volcanic rocks (Wang *et al.*, 2007). According to the research data, there is a north-south-trending uplift in the conductive layer of upper mantle in Tengchong, with 60-90 km buried depth. Along with the uplifting of mantle and the extension of crustal, the crustal materials and mantle magma assimilated other mass in crustal to form magma

chamber at vantage point when erupting upward to the earth surface (Wang *et al.*, 1993).

Many researches have been carried out to study the characteristics of the magma chamber's intrusion in Tengchong. Magnetoelluric (MT) exploration of Tengchong-Lianghe area demonstrated that there is a magma chamber of 5-25 km depth under Rehai area (Bai *et al.*, 1994). After analysis of the 3D seismic velocity tomography of the upper crust in Tengchong, Wang *et al*. (2002) thought there is a magma chamber of 7-14 km depth under Menglian-Tuantian area (Wang *et al.*, 2002).

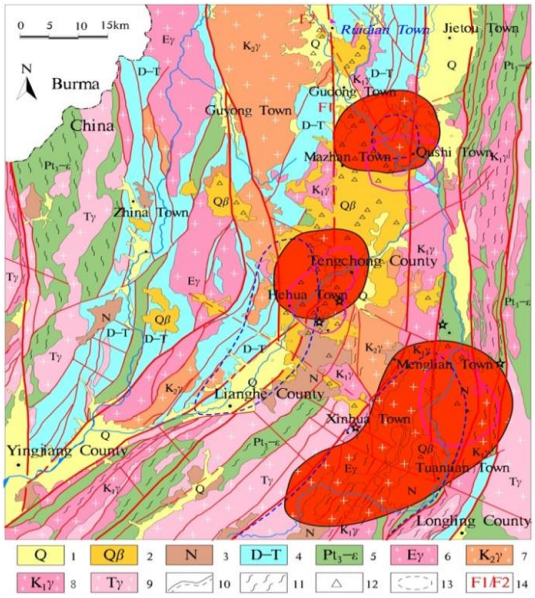

Figure 2. Distribution map of regional geology and Magma chamber: 1-Quaternary sediments; 2-Quaternary volcanic rocks; 3-Palaeogene-Neogene period volcanic sedimentary rocks; 4-Devonian-Triassic; 5-Neoproterozoic-Cambrian; 6-Paleogene granite; 7-Late Cretaceous granite; 8-Early Cretaceous granite; 9-Triassic granodiorite; 10-Measured/predicted fault; 11-Mylonitic foliation; 12-volcanic vent; 13-Geothermal anomaly area; 14-F1: Tengchong-Dayingjiang River Fault, F2: Longchuanjiang Fault; Other: Black solid line reference from the literature (Zhao et al., 2008); Purple solid line reference from the literature (Zhao et al., 2011); Blue dotted line reference from the literature (Jin et al., 2015)

According to the observed earthquake swarm distribution and S-wave annihilation, Ye *et al*. (2003) thought there are two magma chambers in the south to Dayingshan volcano less than 14 km depth. One is of 4-6 km depth between Laoguipo Volcano and Maanshan Volcano. The other one is of 8-14 km depth in Maanshan-Thengchong-Rehai area (Wang *et al.*, 2004). Zhao *et al*. (2006, 2008, 2011, 2012) studied the carbon isotope fractionation of CO_2 and CH_4 gases from hot

springs, the mantle-derived characteristics of He and the relative geothermal gradient in Tengchong volcanic area. They drew the shapes of these three magma chambers and predicted the current temperature of each chamber (Wang *et al.,* 2002; Zhao *et al.,* 2006; Zhao *et al.,* 2008; Zhao *et al.,* 2011; Zhao *et al.,* 2012). The distribution map of regional geology and magma chambers are shown in Figure 2.

3.3. The relationship between magma chambers in Ruidian and Mazhan

Various scholars' researches showed that there are three magma chambers deep under the volcanic basin in Tengchong. The one near high temperature geothermal field in Ruidian is Gudong-Mazhan magma chamber.

In 1980s, MT exploration has been carried out in Mazhan area. Researchers found that an intrusion (5 km thick, 6-10 Ω·m resistivity of conducting layer) is 9-10 km depth and they inferred it should be Mazhan magma chamber (Bai *et al.,* 2002). Tan *et al*. focused on measuring Xiaokongshan-Heikongshan area, which is north of Mazhan, three times in 2010-2011. They used large scale MT method, Controlled-Source Audiomagnetotellurics method and aeromagnetic survey to detect the gravity and seismic reflection profile. The Gudong-Mazhan magma chamber's distribution area and geometric characteristics are reported (Tan *et al.,* 2013). Jiang *et al*. (2012, 2016) also detected the intrusion location of Mazhan magma chamber and its geometry by MT and Controlled-Source Audiomagnetotellurics methods. The magma chamber is under the Xiaokongshan crater, in the south of Mazhan-to the north is Gudong town, to the south is Xiaokongshan, to the east is Qushi township, to the west is western Mazhan (Jiang *et al.,* 2012; Jiang *et al.,* 2016).

The magma chamber of 12-30 km depth in Godong-Mazhan is in the Tengchong Main Fault, and it is once connected with another magma chamber in southern Tengchong (Jiang *et al.,* 2012). In addition, the geophysical research of the volcanic region of northern Thengchong, demonstrated that the magma chamber of in Godong-Mazhan is once connected with the magma chamber in Rehai geothermal field area. They intruded contemporaneous.

The magma chamber in Gudong-Mazhan-qushi area is derived from the magma source of deep mantle. With the strong seismic activities and volcanic activities in Tengchong, the up-mantle materials upwelled through the crust and ground surface. During this process, the magma chamber is melted with curst materials and mainly distributed in up-mantle.

The depth of the top surface of the magma chamber near Heikongshan, Mazhan is 12-13 km. Its east-west axis length is 25 km and is on the east of Dayingjiang Rvier Fault. Its north-south axis length is 30 km. The depth range of this magma chamber is 13-30 km. The temperature range is 397-651 ℃, the highest among which is 700 ℃ (Li *et al.,* 2011; Zhao *et al.,* 2008).

Combining the researches of Zhao (Zhao *et al.,* 2006; Zhao *et al.,* 2008; Zhao *et al.,* 2011; Zhao *et al.,* 2012), Jiang (Jiang *et al.,* 2012; Jiang *et al.,* 2016), Lin (Lin *et al.,* 2005) and Li (Lin *et al.,* 2011), we can probably confirm the geometry of the

magma chamber in Gudong-Mazhan is an approximate ellipsoid with east-west axis length 19 km, north-south exis length 25 km, hight 15 km. The magma chamber is connected with the north forward of Thengchong-Dayingjiang River Fault (F1) and Ruidian-Qushi Fault (F2). Therefore, both Faults are the main structures to conduct and control the heat in Ruidian geothermal field. Moreover, the secondary fault is the secondary structure for heat conduction.

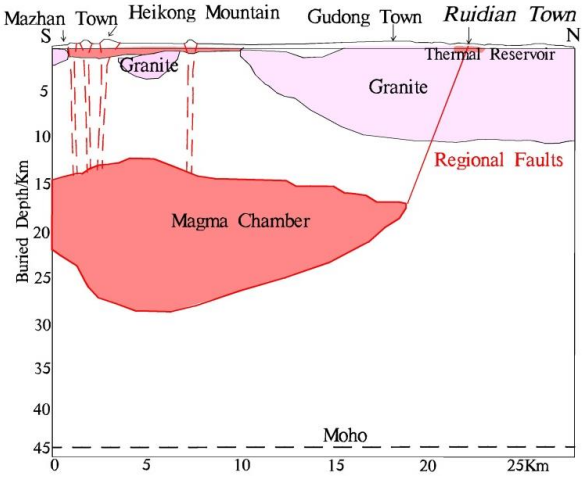

Figure 3. The schematic section of magma chamber in Gudong-Mazhan area (Modified from (Jiang et al., 2012)

4. Redioation characteristics of the biotite adamellite

4.1. Introduction of the radioactive heat generation rare

The heat generated from the decay of radioactive elements determined the temperature distribution in the rocks. The heat flows observed on the ground are crustal heat flow and mantle heat flow. The up crustal heat flow is heated by the decay of ^{238}U, ^{232}Th and ^{40}K in up crustal.

There is a mass of radioactive elements such as Uranium, Thorium and Potassium in granite. ^{235}U, ^{238}U, ^{232}Th and 40K are the natural radioactive nuclides of the longest half-life periods and higher amounts. The half-life periods of ^{235}U, ^{238}U, ^{232}Th and ^{40}K are 7.038×10^8 a, 4.468×10^9 a, 1.41×10^{10} a and 1.28 × 109 a, respectively (Nier *et al.*, 1939). One of the basic properties of the radioactive elements is that they release α, β and γ particles when decaying and the particles convert to heat. The heat released from the radioactive elements in per unit time is called Radioactive Heat Generation Rate (QA).

The heat generation rate constant of natural Uranium (achieving the radioactive equilibrium), Thorium (disintegrated from equilibrium ^{232}Th) and Potassium

(abundance of ^{40}K is 0.0118%) are 9.525 × 10^{-5} w/kg, 2.561 × 10^{-5} w/kg and 3.447 × 10^{-9} w/kg, respectively (Reinhardt *et al.*, 1995; Rybach, 1976; Rybach, 1976). The decaying process and the parameters list of heat convention when decaying of radioactive elements are shown in Figure 4 and Table 1.

$$^{238}_{92}U \xrightarrow{4.47\times10^{9}a} (-8He) \rightarrow {}^{206}_{82}Pb$$

$$^{235}_{92}U \xrightarrow{7.04\times10^{8}a} (-7He) \rightarrow {}^{207}_{82}Pb$$

$$^{232}_{90}Th \xrightarrow{1.41\times10^{10}a} (-6He) \rightarrow {}^{208}_{82}Pb$$

$$^{40}_{19}K \xrightarrow{1.28\times10^{9}a} {}^{40}_{18}Ar$$

Figure 4. The decaying process of radioactive elements

Table 1. The parameters list of heat convention when U and Th decaying

Isotope	**Mass conservation**	**EΔm (MeV)**	**∑Eβmax (MeV)**	**Eabs (MeV)**	**Eabs**
^{238}U	m(U^{238})-8m(He^4)-m(Pb^{206})	51.667	7.99	46.34	47.4
^{235}U	m(U^{235})-7m(He^4)-m(Pb^{207})	46.392	1.71	45.26	45.2
^{232}Th	m(Th^{232})-6m(He^4)-m(Pb^{208})	42.793	5.71	38.99	39.8

Table 2. The heat generation rates of rocks

Type	**Rocks**	**Heat generation rate (μW/m³)**
Igneous rocks	Granite/Rhyolite	2.450
	Granodiorite/Dacite	1.490
	Diorite/Quartz diorite/Andesite	1.080
	Gabbro/Basalt	0.310
	Olivine	0.012
Sedimentary rocks	Limestone	0.620
	Dolomite	0.36
	Quartzite	0.33
	Arkose	0.85
	Shale	1.80
	Deep sea sediments	0.78
Metamorphic rocks	Greenschist/Low amphibolite facies	3.15
	high amphibolite facies	1.17
	low-pressure granulite-facies	0.73
	high-pressure granulite-facies	0.45

In consequence, we can calculate the heat generation rate of rocks of different concentrations of Uranium, Thorium and Potassium. Most of the radioactive elements are in the up crustal. Different rocks had different heat generation rates. The heat generation rate of granite is almost the highest (Table 2).

Previous researches have shown that the decaying heat of radioactive elements is a good condition to form hot springs (Guo *et al.*, 2014; Zhao *et al.*, 2003). Furthermore, the high thermal conductivity of granite makes it easy to deliver the heat from crustal to the ground. This is one of the reasons why hot springs occur in granite areas.

4.2. Chemical characteristics of Granite

According to the formation mechanism types, eras and location distributions of the granites in Tengchong area, we can divide the granites into three belts (Figure 5). From the west to the east, they are Binlangjiang granite belt (66.4-41.2 Ma), Guyong granite belt (84.3-65.9 Ma) and Donghe granite belt (143.0-11.7 Ma), which were forming at Paleogene age (EH), Late Cretaceous (K2) and Early Cretaceous (K2), respectively.

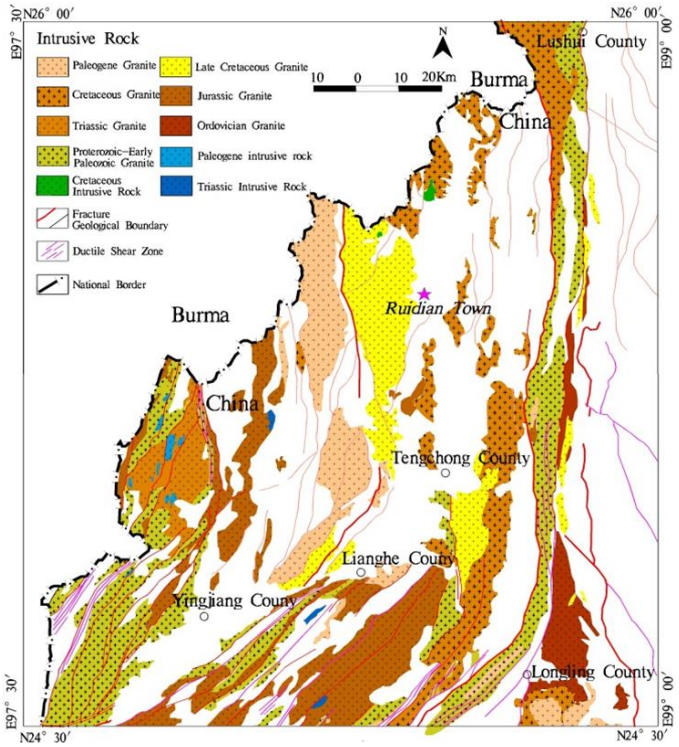

Figure 5. Schematic diagram of magmatic rock and fault distribution in Ruidian area

According to the field survey, the basal of Ruidian area is Guyong granite. The granite's color is grey white or pale red, containing medium-coarse porphyraceous and medium-to-fine-grained structures. The Guyong granite is consist of Potash Feldspar (40-45%), Plagioclase (25-30%), Quartz (20-25%) and Biotite (5-10%). The basal Guyong granites are medium-to-fine-grained Biotite Adamellite and medium-coarse porphyraceous (Biotite) Adamellite. The Potash Feldspar contains Perthite and Microcline, the particle sizes of the medium-coarse porphyraceous and medium-to-fine-grained are 2-6 mm and 1-3 mm, respectively. The Plagioclase is oligoclase and the particle sizes of the medium-coarse porphyraceous and medium-to-fine-grained are 2-5 mm and 1-4 mm, respectively. The Biotite is subhedral plate with particle size 1-3 mm and it is of chloritization and sometimes sericitization. The Quartz is xenomorphic granular with particle size 1-5 mm. The detailed petrography characteristics of granite are shown in Figure 6.

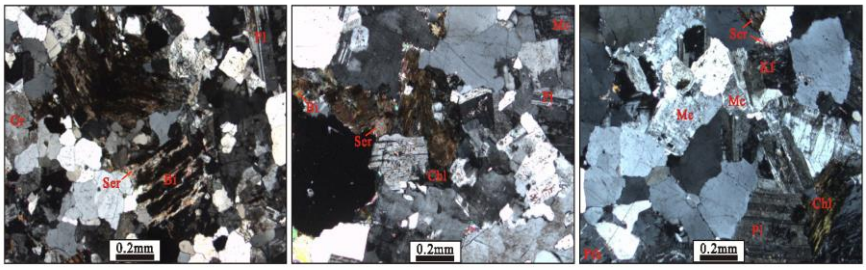

Figure 6. The petrography characteristics of Guyong granite belt (Under Transmission Crossed Polarized Light). Q: Quartz, P1: Plagioclase, Kf: Potash Feldspar, Or: Orthoclase, Mc: Microcline, Pth: Perthite, Bi: Biotite, Ser: Sericitization, Chl: Chloritization.

4.3. Characteristics of granite age

Kinds of methods have been utilized to measure the age of granite, such as LA-ICP-MS, Zircon U-Pb and SHRIMP. Single grained Zircon U-Pb dating obtained that the basal Guyong granite is 76-69 Ma (Yang *et al.*, 2009; Yi *et al.*, 2012). Conventional Zircon U-Pb dating method obtained the granite is 70.3±3.2-75.3±4.2 Ma (Ma *et al.*, 2013). Therefore, we define the granite age in Ruidian geothermal field is between 76-69 Ma.

4.4. Radioactive heat generation rate of granite

The heat generated from radioactive elements' decaying is an important source to form geothermal field (Ingvar, 2001). The granite contains vast of ^{238}U, ^{232}Th and ^{40}K, which can generate heat when they decaying (Hurley, 1953). We can calculate the heat generation rate of granite based on the concentration of ^{238}U, ^{232}Th and ^{40}K.

The radioactive heat generation rate and relative parameters of U, Th and K are listed in Table 3.

Table 3. Radioactive heat generation rate and parameters of U, Th and K

Element	**U**		**Th**	**K**	
Isotope	^{238}U	^{235}U	^{232}Th	^{40}K	
Abundance (%)	99.275	0.720	100	0.0119	
Decay constant	1.551×10^{-10}	9.85×10^{-10}	4.95×10^{-11}	5.53×10^{-10}	
heat generation rate (J/g·a)	2.973	18.003	0.837	0.950	
	2.897	18.171	0.808	0.921	
	2.989	17.960	0.833	0.921	
	Natural Uranium	3.056	0.837	Natural Potassium	1.130
		3.006	0.808		1.096
		3.098	0.833		1.096

Researches usually use the following equation to calculate the radioactive heat generation rate (Birch *et al.,* 1954; Elsaid *et al.,* 2014; Dini *et al.,* 2005; Hady *et al.,* 1994; Singh *et al.,* 2009; Tucker *et al.,* 2013; Wu *et al.,* 2005):

$$Q_A(\mu W / m^3) = 0.01\rho(9.52C_U + 2.56C_{Th} + 3.48C_K) \quad (1)$$

where C_U, C_{Th} and C_K are the concentrations of U, Th and K in the granite, respectively. The unit of C_U and C_{Th} is 10^{-6} while C_K are is 10^{-2}, ρ is the granite density (g/cm^3).

According to the parameters in Table 3, we derived three calculation equations of radioactive heat generation rate below:

$$Q_A(\mu J / g \cdot a) = 3.098C_U + 0.833C_{Th} + 1.097C_K) \quad (2)$$

$$Q_A(HGU) = 0.317\rho(0.74C_U + 0.199C_{Th} + 0.262C_K) \quad (3)$$

$$Q_A(\mu W / m^3) = 0.01\rho(9.82C_U + 2.64C_{Th} + 3.48C_K) \quad (4)$$

where C_U, C_{Th} and C_K are the concentrations of U, Th and K in the granite, respectively. ρ is the granite density (g/cm^3). HGU is the unit of radioactive heat generation rate (1 HGU = 4.1868×10^{-7} J/m^3·s or 1×10^{-13} cal/cm^3·s).

Uranium and Thorium in the nature almost exist as ^{238}U and ^{232}Th. The relative atom mass of Oxygen and Potassium in K_2O are 15.999 and 39.098, respectively. The mass fraction of Potassium can then be calculated as 39.098 × 2/(39.098 × 2 + 15.999) = 0.829787. The mass of Potassium can be represented as 0.829787× K_2O,

or the mass of K_2O can be represented as 1.205128× K. Combining with Equation 1, we applied Equation 5 for calculation in our research:

$$Q_A(\mu W/m^3) = 0.01\rho(9.52C_U + 2.56C_{Th} + 2.88C_{K2o}) \quad (5)$$

where Q_A is the heat generation rate of radioactive element (unit: μW/m3); C_U (μg/g), C_{Th} (unit: μg/g) and CK (unit: %) are the abundances of ^{238}U, ^{232}Th and K_2O; ρ is the granite density (g/cm^3).

The average density of Guyong granite is 2.62 g/cm^3. Combining with the composition analysis table, we listed the Q_A of Guyong granite in Table 4. Comparing to the heat generation rates of other granites in other places of the world (Table 5), The Q_A of 6.90 μW/m^3 is abnormally high. The heat generation rates of granites in different areas are listed in Table 5 (Zou *et al.*, 2010; Mareschal *et al.*, 2004).

When the heat generation rate is constant, we take it into consideration that K is dependent on temperature: If T <300℃, a = 0.001 (1/℃). Then the analytical solution of one-dimensional heat conduction equation is (Wang *et al.*, 2001):

$$T(z) = \left(\frac{1}{a}\right)\left\{(1+aT_0)\exp\left[\left(\frac{a}{K_0}\right)(q_0 z - Az^2)\right] - 1\right\} \quad (6)$$

If $A(z) = A_0\exp(-z/D)$, K is a constant, the analytical solution of one-dimensional heat conduction equation is:

$$T(z) = T_0 + \frac{q_0}{K}z + \frac{A_0 D}{K}\exp\left(-\frac{z}{D}\right)z + \frac{A_0 D^2}{K}\left[1 - \exp\left(-\frac{z}{D}\right)\right] \quad (7)$$

where D = 1/e (e = 2.71828) is the decay factor of heat generation rate.

Table 4. Radioactive heat generation rates (QA) of granites in Ruidian area

No.	Sampling spot	K_2O (%)	U (ppm)	Th (ppm)	QA (μW/m^3)
RD01	Guyong granite	5.05	13.2	59.6	7.67
RD02	Guyong granite	5.27	14.2	57.9	7.82
RD03	Guyong granite	5.30	12.4	45.7	6.56
RD04	Guyong granite	5.23	11.8	43.8	6.28
RD05	Guyong granite	5.01	11.8	46.2	6.42
RD06	Guyong granite	5.31	12.3	48.7	6.73
RD07	Guyong granite	5.10	12.5	50.7	6.90
RD08	Guyong granite	5.29	11.7	48.7	6.58
Average					6.90

Table 5. The statistics of heat generation rates of granites in different areas in the world

Producing Area	Rock Name	Heat Generation Rate ($\mu W/m^3$)
China	Baoshan rock	5.60
China	Jiuhuashan rock	6.80
China	Fogang rock	6.70
China	Dadongshan rock	6.70
France	Central massif rock	5.25
Switzerland	Mittagfluh granite	6.60
USA	Eastern rock in Wyoming State	4.56
Canada	Manitou lake rock	2.10

If $A(z)$ decreases exponentially, and K is dependent on temperature, the analytical solution of one-dimensional heat conduction equation is [48]:

$$T(z)=\left(\frac{1}{a}\right)\left\{(1+aT_0)\exp\left\{\left(\frac{a}{K_0}\right)\left[(A_0D^2)\left(1-\exp\left(-\frac{z}{D}\right)\right)+q_0z-A_0Dz\right]\right\}-1\right\} \quad (8)$$

where T_0 is the mean surface temperature or specific reference temperature, z is the depth, $q0$ is the earth surface heat flow, K is the thermal conductivity of granite, A is the heat generation rate of granite, D is the thickness of the radioactive elements enrichment-layer, A_0 is the heat generation rate of the exposed granite. The thermal conductivity of granite in Ruidian area K = 2.64 J/m·s·℃, the average A = 6.90 $\mu W/m^3$, D = 10 km. We can calculate the q_0 = 122 mW/m^2.

Equations 7 and 8 were used to calculate the temperature of z = 2000 m, and the $T(2000)$ were 120 and 116 ℃, respectively. The results indicated that the heat generation rate of granite is very important to the earth surface temperature. This also can explain the reason why hot springs in granite areas with low earth heat flow values. In this paper, the above earth surface temperature calculations didn't consider the afterheat of magma chambers, the heat conductions of Tengchong-Dayingjaing River Fault and Ruidian-Qushi Fault.

5. Heat source conditions of the geothermal field

Previous research achievements had determined the magma chamber of 12-30 km depth. The depth of the top surface of the magma chamber near Heikongshan is 12-13 km. Its east-west axis length is 25 km and is on the east of Dayingjiang Rvier Fault. Its north-south axis length is 30 km. The depth range of this magma chamber is 13-30 km. The high temperature range is 651-700 ℃. This magma chamber's resistivity is low and the resistivity of electrical conducting layer is 6-10 Ω·m. It is This magma chamber that formed the high temperature geothermal field in Ruidian area.

Ruidian area is about 10 km to the north of Gudong-Mazhan area, and the geothermal field is under the north section of Tengchong-Lianghe Fault (F1), which is a large thermal active fault belt area. The secondary fault belt is Ruidian-Qushi Fault (F2). Tengchong-Dayingjiang River Fault (F1) cutting is very deep and it serves as the channel to conduct heat from magma chamber in Gudong-Mazhan to high temperature geothermal field in Ruidian (Figure 7).

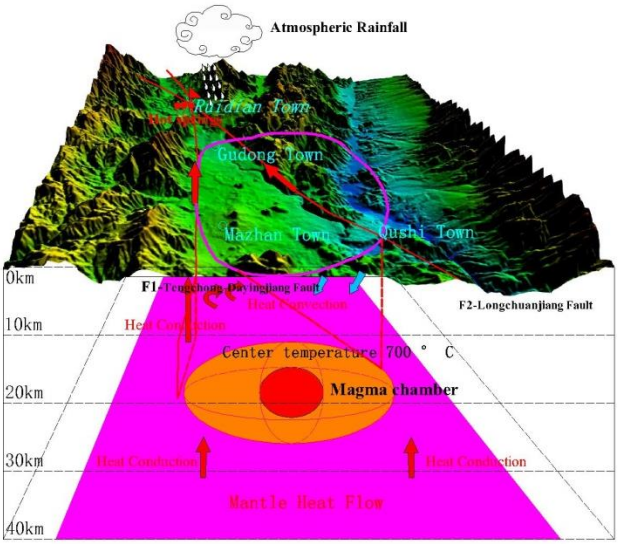

Figure 7. The heat generation model of geothermal field in Ruidian area

In addition, the average heat generation rate of granite is 6.90 μW/m^3, which is relatively high in the world. The basal biotite adamellite is rich in ^{238}U, 232Th and 40K redioactive elements. The estimated temperature is 116-120 °C in 2 km depth. The rediation heat has a vital impact on ground temperature field's distribusion in Ruidian area.

The main geological structure of the geothermal field is fault belts. The north-south fault is the main fault, and the east-west fault is the secondary fault. These faults are not only of large scales, far extension, but also deep cutting. Even some are ultracrustal deep faults. The large-scale faults make the surrounding rocks fractures growth to increase the water conductivity and abundance. The meteoric water seeps through the faults and heated by the magma chamber, then rises along the fault to the heat reservoir layer. Part of the heat water passes through the fractures in the weak regions of the caprock, comes out the ground surface as hot springs. Therefore, the large-scale faults not only control the formation and distribution of the stratums and volcanoes, but also serve as the channel to connect the magma chamber and the deep reservoir. The heat generation model of geothermal field in Ruidian area is shown in Figure 7.

6. Conclusions

1. A magma chamber of 6-10 Ω·m resistivity in the upper crust electrical conducting layer near Gudong-Mazhan area, southern of Ruidian geothermal field. The magma chamber intruded in the late Pleistocene era. The up-boundary is 12-13 km deep. Its geometrical shape is an approximate ellipsoid with east-west axis length 19 km, north-south exis length 25 km, hight 15 km. The current temperature ranges of 651-700 °C.

2. Ruidian geothermal field is located in the north section of Tengchong-Lianghe Fault (F1), which is a large geothermal active area. Ruidian-Qushi Fault (F2) is a secondary fault. Tengchong-Lianghe Fault is a deep fault that can be the heat transportation channel for magma chamber from Dudong-Mazhan area. In other words, magma chamber from Dudong-Mazhan area is the main heat source of high temperature geothermal field in Ruidian.

3. The basement of Ruidian geothermal field is biotite adamellite, which is the product of volcanic activities in Late Yanshanian. The average rate of heat generation of the monazite is 6.90 μW/m^3. The Paleobiotite monazite is rich in ^{238}U, ^{232}Th and ^{40}K. The rediation heat from the monazite keeps the estimated temperature ranges of 116-120 °C in 2 km buried depth. The rediation heat is an important heat source to form geothermal field in Ruidian and has a vital impact on ground temperature field's distribusion.

Acknowledgment

This work was supported by the National Natural Science Foundation of China (No. 41502342) and the Geological survey project of China (No. DD20160303).

References

Bai D. H., Liao Z. J. (1994). Inferring the magma heat source of the Tengchong Hot Sea Thermal Field from the results of MT detection. *Chinese Science Bulletin*, Vol. 39, No. 4, pp. 344-347

Birch F. (1954).Heat flow radioactivity. Faul H. Nuclear Geology. *New York :John Wiley & Son*, pp. 154-185

Dini A., Gianelli G., Puxeddu M. (2005). Origin and evolution of pliocene-pleistocene granites from the larderello geothermal field (tuscan magmatic province, Italy). *Lithos*, Vol. 81, No. 1, pp. 1-31. https://doi.org/10.1016/j.lithos.2004.09.002

Elsaid M., Aboelkhair H., Dardier A. (2014). Investigation of a relation between radiogenic heat production and kinetic surface temperature from multispectral aster-tir data: a case study on elmissikat-eleridiya granites, central eastern desert, Egypt. *Arabian Journal of Geosciences*,Vol. 7, No. 11, pp. 4615-4628. https://doi.org/ 10.1007/ s12517 -013-1118-8

Guo Q. H. (2012). Hydrogeochemistry of high-temperature geothermal systems in China: A review. *Applied Geochemistry*, Vol. 7, No. 10, pp. 1887-1898. http://dx.doi.org/10.1016/j.apgeochem.2012.07.006

Guo Q. H., Liu M., Li J. (2014). Acid hot springs discharged from the Rehai hydrothermal system of the Tengchong volcanic area (China): Formed via magmatic fluid absorption or geothermal steam heating? *Bulletin of Volcanology*, Vol. 76, No. 10, pp. 868. https://doi.org/10.1007/s00445-014 -0868-9

Guo S. Y., Li X. J. (2013). Reservoir stratum characteristics and geothermal resources potential of Rongcheng uplift geothermal field in Baoding, Hebei. *Chinese Journal of Geology*, Vol. 48, No. 3, pp. 922-931. http://dx.doi.org/10.3969/j.issn.0563-5020.2013.03.026

Hady E. E. A., El-Sayed A. M. A., Ahmed A. A. (1994). Natural radioactivity of basement younger granite rocks from the eastern desert. *Radiation Physics & Chemistry*, Vol. 44, No. 1, pp. 223-224. https://doi.org/10.1016/0969-806X(94)90136-8

Hurley P. M., Fairbairn H. W. (1953). Radiation damage in Zircon: A possible age method. *Geological Society of America Bulletin*, Vol. 64, No. 6, pp. 659-673. http://dx.doi.org/10.1130/ 0016-7606(1953)64[659:RDIZAP]2.0.CO;2

Ingvar B. F. (2001). Geothermal energy for the benefit of the people. *Renewable and Sustainable Energy Reviews*, Vol. 16, No. 3, pp. 299-312. http://dx.doi.org/10.1016/S1364-0321 (01)00002-8

Jiang M., Tan H. D., Peng M. (2016). A further discussion on geophysical characteristics of Mazha. *Geology in China*, Vol. 43, No. 5, pp. 1688-1696

Jiang M., Tan H. D., Zhang J. W. (2012). Geophysical mode of mazhan-gudong magma chamber in tengchong volcano-tectonic area. *Acta Geoscientica Sinica*, Vol. 33, No. 5, pp. 731-739. https://doi.org/10.3975/cagsb.2012.05.03

Khair H. A., Cooke D., Hand M. (2015). Seismic mapping and geomechanical analyses of faults within deep hot granites, a workflow for enhanced geothermal system projects. *Geothermics*, Vol. 53, No. 53, pp. 46-56. https://doi.org/10.1016/j.geothermics.2014.04.00 7

Li H., Peng S. B., Qiao W. T. (2011).The distribution and activity of Cenozoic magma chamber in Tengchong volcano area deduced from the MODIS multi-temporal monthly night LST data. *Acta Petrologica Sinica*, Vol. 27, No. 10, pp. 2873-2882. https://doi.org/1000-0569/2011/027(10)-2873-82.

Lin M. S., Peng S. B., Qiao W. T. (2014). Petro-geochemistry and geochronology of late Cretaceous-Eocene granites in high geothermal anomaly areas in the Tengchong block,Yunnan Province, China and their tectonic implications. *Acta Petrologica Sinica*, Vol. 30, No. 2, pp. 527-546. https://doi.org/1000-0569 /2014 /030(02) -0527-46

Ma L., Deng J., Wang Q. F. (2013). Geochronology of the Dasongpo tin deposit, Yunnan Province: Evidence from zircon LA-ICP-MS U-Pb ages and cassiterite LA-MC-ICP-MS U-Pb age. *Acta Petrologica Sinica*, Vol. 29, No. 4, pp. 1223-1235. https://doi.org/1000-0569/2013/029(04)-1223-35

Mareschal J. C., Jaupart C. (2004). Variations of surface heat flow and lithospheric thermal structure beneath the north american craton. *Earth & Planetary Science Letters*, Vol. 223, No. 1, pp. 65-77. https://doi.org/10.1016/j.epsl.2004.04.002

Nier A. O. (1939).The Isotopic Constitution of Radiogenic Leads and the Measurement of Geological Time. II. *Phys Rev* ,Vol. 55, No. 2, pp. 153-163. https://doi.org/10.1103/PhysRev.55.153

Pang Z. H., Hu S. B., Wang J. Y. (2012). A roadmap to geothermal energy development in China. *Science&Technology Review*, Vol. 30, No. 32, pp. 18-24. http://dx.doi.org/10.3981/j.issn. 1000-7857. 2012.32.002

Piña-Varas P., Ledo J., Queralt P. (2014). 3-D magnetotelluric exploration of tenerife geothermal system (Canary Islands, Spain). *Surveys in Geophysics*, Vol. 35, No. 4, pp. 1045-1064. http://dx.doi.org/1045-1064. 10.1007/s10712-014-9280-4

Rybach L. (1976). Radioactive heat production in rocks and its relation to other petrophysical parameters. *Pure and Applied Geophysics*, Vol. 114, No.2,pp. 309-317. https://doi.org /10.1007/BF00878955

Rybach L. (1976). Radioactive heat production: A physical property determined by the chemistry of rocks. In: Sterns RGJ (ed) The physics and chemistry of minerals and rocks. *Wiley, New York*. pp. 309-318.

Singh A. K., Vallinayagam G. (2009). Radioactive element distribution and rare-metal mineralization in anorogenic acid volcano-plutonic rocks of the neoproterozoic malani felsic province, western peninsular india. *Journal of the Geological Society of India*, Vol. 73, No. 6, pp. 837-853. https://doi.org/10.1007/s12594-009-0067-z

Tan H. D., Jiang M., Lin C. H. (2013). Characteristics of electrical structure of Tengchong volcano-tectonic belt in Yunnan Province. *Geology in China*, Vol. 40, No. 3, pp. 800-806

Tenzer H., Park C. H. (2010). Application of the geomechanical facies approach and comparison of exploration and evaluation methods used at Soultz-sous-Forts (France) and Spa Urach (Germany) geothermal sites. *Environmental Earth Sciences*, Vol. 61, No. 4, pp. 853-880. http://dx.doi.org/10.1007/s12665-009-0403-z

Tucker R. T., Zou H., Fan Q. (2013). Ion microprobe dating of zircons from active dayingshan volcano, tengchong, se tibetan plateau: time scales and nature of magma chamber storage. *Lithos*, Vol. 173, No. 4, pp. 214-221. https://doi.org/10.1016/j.lithos.2013.04.017

Wang C. Y., Lou H., Wu J. P. (2002).Seismological study on the crustal structure of tengchong volcano-geothermal area. *Acta Seismologica Sinica*, Vol. 24, No. 3,pp. 231-242.

Wang C. Y., Huangfu G. (2004). Crustal structure in tengchong volcano-geothermal area, western Yunnan, China. *Tectonophysics*, Vol. 380, No. 1, pp. 69-87. https://doi.org/10.1016/ j.tecto.2003.12.001

Wang G. L., Zhang F. W., Liu Z. M. (2000). An analysis of present situation and prospects of geothermal energy development and utilization in the world. *Acta Geoscientia Sinica*, Vol. 21, No. 2, pp. 134-139. http://dx.doi.org/10.3321/j.issn: 1006-3021.2000.02.004

Wang J. Y., Hu S. B., Cheng B. H. (2001). Predication of the deep temperature in the target area of the china continental scientific drilling. *Chinese Journal of Geophysics*, Vol. 44, No. 6, pp. 774-782

Wang Y., Zhang X., Jiang C. (2007). Tectonic controls on the late Miocene-Holocene volcanic eruptions of the Tengchong volcanic field along the southeastern margin of the Tibetan plateau. *Journal of Asian Earth Sciences*, Vol. 30, No. 2, pp. 375-389. https://doi.org/10.1016/ j.jseaes.2006.11.005

Wang X. B., Xu S., Chen J. F. (1993). Characteristics of hot gas components and strontium isotopes in the Tengchong volcanic area. *Chinese Science Bulletin*, Vol. 38, No. 9, pp. 814-817.

Wilson C. K., Jones C. H., Gilbert H. J. (2003). Single-chamber silicic magma system inferred from shear wave discontinuities of the crust and uppermost mantle, Coso geothermal area, California. *Journal of Geophysical Research Atmospheres*, Vol. 108, No. 5, pp. 937-951. https://doi.org/10.1029/2002JB001798

Wu Y., Jin Z. M., Ou X. G. (2005). Lithospheric thermal structure beneath the area of the Chinese Continental Scientific Drilling Site (CCSD). *Acta Petrologica Sinica*, Vol. 21, No. 2, pp. 439-450. https://doi.org/1000-0569/2005/021(02)-0439-50

Xu Q., Li C. H., Wang J. A. (1997). Geothermal resources in tengchong region, Yunnan province. *Geology-geochemistry*, Vol. 4, pp. 77-84.

Yang Q. J., Xu Y. G., Huang X. L. (2009). Geochronology and geochemistry of granites in the Tengliang area, western Yunnan: Tectonic implication. *Acta Petrologica Sinica*, Vol. 25, No. 5, pp. 1092-1104. https://doi.org/1000-0569 /2009 /025(05) -1092-04

Yi G. X., Qi J. Y., Jiang B. L. (2012). Temporal-spatial distribution and tectonic implications of the batholiths in the Gaoligong-Tengliang-Yingjiang area, western Yunnan: Constraints from zircon U-Pb ages and Hf isotopes. *Journal of Asian Earth Sciences*, Vol. 53, No. 1, pp. 151-175. https://doi.org/10.1016/j.jseaes.2011.06.018

Zeng H. Y., Diao N. R., Fang Z. H. (2010). A *finite* line-source model for boreholes in geothermal heat exchangers. *Heat Transfer-asian Research*, Vol. 31, No. 7, pp. 558-567. http://dx.doi.org/10.1002/htj.10057

Zhao C. P., Ran H., Chen K. H. (2011). Present-day temperatures of magma chambers in the crust beneath tengchong volcanic field,southwestern china:estimation from carbon isotopic fractionation between co_2 and ch_4 of free gases escaped from thermal springs. *Acta Petrologica Sinica*, Vol. 27, No. 1, pp. 2883-2897. https://doi.org/1000-0569/2011/027(10)-2883-97

Zhao C. P., Ran H., Chen K. H. (2006). Present-day magma chambers in Tengchong volcano area inferred from relative geothermal gradient. *Acta Petrologica Sinica*, Vol. 22, No. 6, pp. 1517-1528. https://doi.org/1000-0569 /2006/022(06)-1517-28

Zhao C. P. (2008). Characteristics of modern mantle derived helium and deep magmatic activity in Tengchong volcanic area. Beijing: Institute of geology, *China Earthquake Administration*, pp. 78-102.

Zhao C. P., Ran H., Wang Y. (2012). Present-day mantle-derived helium release in the Tengchong volcanic field, Southwest China: Implications for tectonics and magmatism. *Acta Petrologica Sinica*, Vol. 28, No. 4, pp. 1189-1204. https://doi.org/1000-0569 /2012/028(04)-1189-04

Reinhardt H. G., Gast H. (1995). The importance of radioactivity in geoscience and mining. *Cellular & Molecular Life Sciences Cmls*, Vol. 51, No. 7, pp. 703-709. https://doi.org/10.1007/BF01941267

Zhao P., Duo J., Xie E. J. (2003). Strontium isotope data for thermal waters in selected high-temperature geothermal fields, China. *Acta Petrologica Sinica*, Vol. 19, No. 3, pp. 569-576. https://doi.org/1000-0569/2003/019(03)-0569-76

Zhou Z. (1997). Study on deep heat flow in Yunnan, China. *Northwestern Seismological Journal*, Vol. 4, pp. 51-57.

Zhou Z. H., Xiang C. Y. (1997). Distribution of the lithospheric geotemperature in Yunnan. *Seismology and Geology* ,Vol. 19, No. 3, pp. 227-234

Zou H., Fan Q., Schmitt A. K. (2010). U-th dating of zircons from holocene potassic andesites (maanshan volcano, tengchon, se tibetan plateau) by depth profiling: time scales and nature of magma storage. *Lithos*, Vol. 118, No. 1, pp. 202-210. https://doi.org/10.1016/j.lithos.2010.05.001